Interior Tomography Approach for MRI-guided Radiation Therapy

Xun Jia and Steve B. Jiang
Department of Radiation Oncology, University of Texas Southwestern Medical Center, Dallas, TX 75390
Email: Xun.Jia@UTSouthwestern.edu, Steve.Jiang@UTSouthwestern.edu

Gary Pickrell
Department of Materials Science and Engineering, Virginia Tech
Blacksburg, VA 24061
Email: pickrell@vt.edu

Ge Wang
Department of Biomedical Engineering, Rensselaer Polytechnic Institute
Troy, NY 12180
Email: wangg6@rpi.edu

***Abstract*—Image guidance plays a critical role in radiotherapy to ensure treatment accuracy. Cone-beam CT (CBCT) installed on a medical linear accelerator (LINAC) is routinely used in clinics for this purpose. While CBCT can provide an x-ray attenuation image to guide patient positioning, low soft-tissue contrast affects the delineation of anatomical features, hindering setup accuracy in many cases. To solve this problem, several MRI-LINAC systems have been developed to combine a full diagnostic MRI scanner with a radiotherapy machine. In this paper, we present a new concept for the development of the MRI-LINAC system. Instead of combining a full MRI scanner with the LINAC, we propose to use an interior MRI (iMRI) approach to image a specific region of interest (ROI) containing the radiation treatment target. The iMRI will offer local imaging of high soft-tissue contrast for tumor delineation. Meanwhile, megavoltage CBCT currently available on the LINAC will be used to deliver a global image of the patients anatomy. This paper describes a top-level iMRI system design and its integration to an LINAC platform. Preliminary studies on magnetic field design and imaging capability are also presented.**

I. Introduction

In cancer radiotherapy, it is of critical importance to precisely deliver a potent amount of radiation dose to the cancerous target, while sparing nearby normal organs to avoid complications. Image guidance is an important step to ensure treatment accuracy. Before a treatment delivery, Image Guided Radiation Therapy (IGRT) first acquires a scan of the patient's anatomy at the day of treatment. The patient is then accurately positioned based on the internal anatomy with respect to the radiotherapy beam as designed in the treatment plan. Modern radiotherapy approaches have made image guidance increasingly important. For instance, the use of novel therapeutic delivery methods such as intensity modulated radiation therapy (IMRT) [1], as well as treatment modalities such as proton and heavy ion therapy [2], have enabled dose distributions that are extremely conformal to the target, but at the same time, vulnerable to positioning errors. In these scenarios, a small spatial misalignment between the target and the radiotherapy beam could potentially cause a large drop in tumor coverage and/or substantially increased normal tissue dose.

Over the years, kilo-voltage Cone-beam CT (CBCT) installed on a medical linear accelerator (LINAC) has evolved to be the most widely used image-guidance tool in radiotherapy [3]. While its value in terms of ensuring setup accuracy have been repeatedly demonstrated by many studies, the predominant role of CBCT in IGRT has been challenged by Magnetic Resonance Imaging (MRI) due to the advantages of superior image contrast, the absence of ionizing radiation, and the potential of functional imaging. Yet, MRI-guided radiation therapy (MRgRT) requires the integration of an MRI scanner on a LINAC platform. This is a challenging engineering problem because of the sharp conflicts between the two devices in terms of physics and geometry. First, a strong magnetic field required by the MRI affects many electronic components inside the LINAC that are susceptible to electromagnetic interference. Second, a conventional MRI system employs a bulky and complex design to realize a sufficiently large field of view (FOV), hindering integration into a space-limited LINAC platform.

Despite the challenges, tremendous progress has been made by many groups towards the integration of MRI with a radiotherapy machine. Nonetheless, attempts to resolve electromagnetic interference between MRI and LINAC under a tight geometry constraint led to systems with suboptimal or compromised functions at an increased cost. For instance, the commercially available system from ViewRay Inc. [4] combined a low-field (0.3 T) MRI and a low-energy Co-60 therapy machine, which is not ideal for treating deeply seated tumors. In the Elektas prototype system [5] (and in other similar systems [6], [7]) integrating a 1.5 T MRI and a LINAC, the bulky design prohibited LINAC couch rotation. This reduced the freedom to develop a high quality treatment plan in some cases, e.g., head-and-neck tumors and stereotactic body radiotherapy. Moreover, all the existing MRI-LINAC systems employed specifically designed LINACs and were incompatible with traditional LINACs. Clinical adoption of these systems has to absorb a high cost burden of the new system development and facility deployment. For those clinics that already have LINACs installed, purchasing a new and expensive MRI-LINAC is a particular concern.

Existing efforts have exclusively focused on combining a full diagnostic MRI system with a radiotherapy machine. Recently, advancements in the interior tomography field have enabled theoretically exact and numerically stable reconstruc-

DOI: 10.12059/Fully3D.2017-11-3111004

tion of an image in an interior region of interest (ROI) [8]. The ROI can be made small but sufficient for clinical applications. Motivated by this advancement, in this paper, we propose a new concept for the development of an MRI-LINAC system. Instead of combining a full MRI scanner and a LINAC, we plan to employ an interior MRI (iMRI) approach that images a local ROI of the most radio-therapeutic relevance, aided by a megavoltage (MV) CBCT image as a complementary global anatomical prior. In this approach, the small ROI will only require a homogeneous magnetic field just enough to cover it. Hence, technical requirements on hardware and compatibility with an LINAC could be relaxed. It is potentially possible to achieve a compact MRI design that is geometrically and electromagnetically compatible with the current LINAC systems. Such an iMRI system may be retrofitted to any LINAC system to enable MRgRT.

II. Method

A. iMRI system and its integration with a LINAC

1) iMRI system: The main hardware component for the proposed iMRI system is illustrated in Fig. 1. The top and bottom superconducting magnets provide the main field $B_0 \sim 0.5\ T$ inside the imaging field of view (FOV) of a diameter $\sim 15\ cm$. The separation between the two magnets is expected to be $\sim 70\ cm$, which should provide enough space to accommodate a typical patient. This can be achieved by designing the current pattern within the superconducting coil systems using standard optimization techniques [9]. A superconducting magnet typically contains cables made of a superconducting material. The cable has to be cooled to below the critical temperature to maintain its superconducting state. Conventionally, this is achieved through the use of a cryostat. The big size and complexity impede the integration of the MRI device to an LINAC gantry. Here, we propose to use superconducting fibers as an alternative to construct the magnet [10]. These superconducting fibers are fabricated to contain a space allowing injection of liquid helium. After injection, fibers can be maintained in the superconducting state for an extended time period for MRI data acquisition, before being heated to the critical temperature [11]. This property is critical in terms of achieving a light weighted iMRI system suitable for mounting to the LINAC gantry, as it may eliminate the need for a cryostat in the superconducting magnet.

For volumetric imaging purpose, the iMRI system will also contain coils to generate gradient magnetic fields along x, y, and z directions. The y gradient can be formed using gradient coils located inside in the superconducting magnets. At the inner surfaces of the two superconducting magnets are x- and z-gradient coils that provide magnetic fields with a constant gradient along the x and z directions, respectively. These two gradient fields are achievable, as having been demonstrated in commercially available open MRI systems. Fig. 1 just draw coils to illustrate our idea. The exact wire winding pattern suitable for iMRI imaging has to be designed following standard techniques.

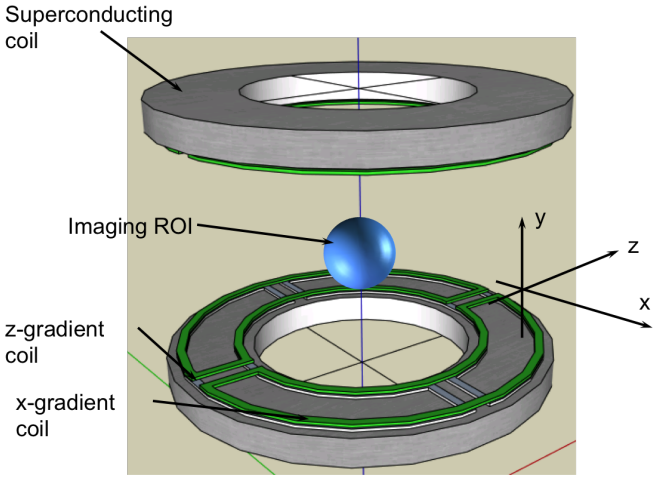

Fig. 1. Illustration of the design of the iMRI device with major components displayed.

2) Integrated iMRI and LINAC: We aim at a compact design, such that the iMRI device can be mounted on the LINAC gantry, as illustrated in Fig. 2(a). The holes on the superconducting magnets allow the radiotherapy beam to pass through. Hence, the electronic portal imaging device (EPID) available on the current LINAC can still receive photon beams from the LINAC, which allows acquisition of portal images. After a full gantry rotation, this setup enables MV CBCT data acquisition to obtain a global view of the patient anatomy complementing the interior MR image inside the ROI.

Due to the compact design, this system still allows radiotherapy treatments conducted at different combinations of the gantry and the couch angles, preserving non-coplanar radiotherapy treatment delivery to a large extent. This is a desired feature, as non-coplanar treatments are advantageous in many cases in terms of reducing normal tissue doses. Three examples of system geometry with different gantry and couch angle combinations are illustrated in Fig. 2(b)-(d).

B. MRI data acquisition and reconstruction

1) Data acquisition: The proposed iMRI system will perform data acquisition similar to a standard MRI system. However, the homogeneous main field B_0 that exists only in the small ROI creates an additional issue that has to be considered. We plan to use the standard slice selection technique by applying a slice selection z-gradient field. The other two gradient fields will be used for frequency encoding and phase encoding. Suppose we are interested in a slice orthogonal to the z axis with a coordinate $z = z_0$, a radio frequency (RF) pulse with frequency $f_0 = \gamma(B_0 + z_0 G_z)$ should be used, where G_z is the gradient amplitude. However, this pulse will in fact excite all points in a set $\Omega = \{(x, y, z) : \gamma[B_0(x, y, z) + zGz] = f_0\}$, not only the targeted slice inside the ROI. Hence, at the moment

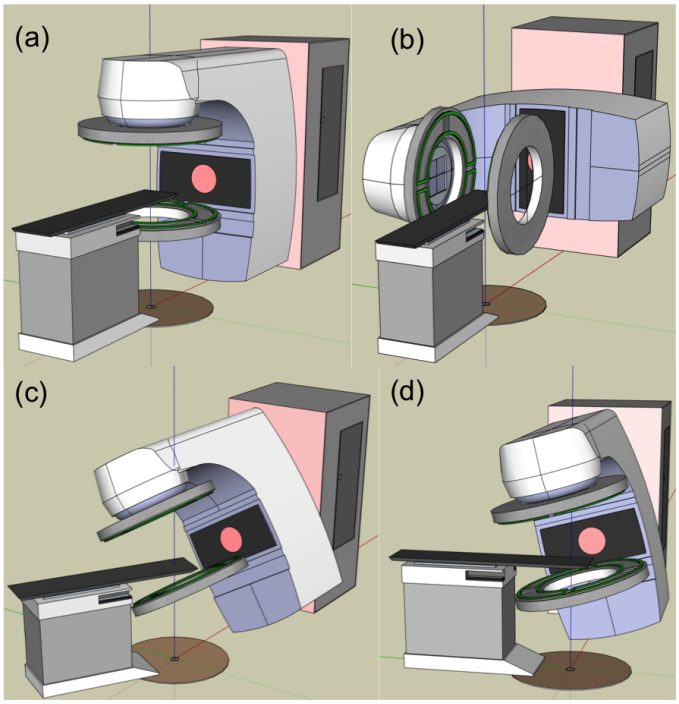

Fig. 2. Geometry relationship between the iMRI and the LINAC .

of measurement, the signal after demodulation is

$$\begin{aligned} S(k_x,k_y) &= \int_{\Omega} \mathrm{d}x\mathrm{d}y\mathrm{d}z\ M(x,y,z)\mathrm{e}^{-\mathrm{i}(k_x x+k_y y)}, \\ &= \int \mathrm{d}x\mathrm{d}y\mathrm{e}^{-\mathrm{i}(k_x x+k_y y)} \int_{\Omega_{(x,y)}} \mathrm{d}z M(x,y,z), \\ &\equiv \int \mathrm{d}x\mathrm{d}y\mathrm{e}^{-\mathrm{i}(k_x x+k_y y)} \hat{M}(x,y). \end{aligned} \quad (1)$$

where $M(x,y,z)$ is the 3D magnetization distribution. $\Omega_{(x,y)}$ is a subset of Ω, namely the intersection between Ω and a straight line that is parallel to the z axis and passing through the point (x,y,z_0). This indicates that the measured signal is equivalently generated from an 2D image $\hat{M}(x,y) = \int_{\Omega_{(x,y)}} \mathrm{d}z M(x,y,z)$. This indeed creates an issue that requires a special attention. For a coordinate (x,y) that is inside the ROI, $\Omega_{(x,y)}$ certainly contains the point (x,y,z_0) due to the set up with a homogeneous B_0 field and a slice selection gradient field. Hence, the measured signal contains contributions from the selected slice at z_0 inside the ROI. However, if $\Omega_{(x,y)}$ also contains points with other z coordinates, the integration along the z axis will mix signals at those z coordinates with that at z_0. In this case, the targeted signal cannot be easily distinguished from other mixed signals, deteriorating image accuracy inside the ROI. This problem can be avoided by carefully designing the magnetic field B_0, such that the aforementioned condition is not satisfied and hence $\hat{M}(x,y) = M(x,y,z_0)$ inside the ROI.

2) Image reconstruction: With the measurement $S(k_x,k_y)$ made, standard reconstruction techniques using analytical reconstruction or iterative reconstruction techniques apply. For radiotherapy online imaging applications, data acquisition time is a critical concern. Therefore, k-space data undersampling is desired to speed up the data acquisition process. In this case, iterative reconstruction will be advantageous, as analytical reconstruction techniques are more vulnerable to image artifacts caused by the data undersampling.

Let us represent the magnetization by a vector u. After discretizing Eq. (1), we arrive at a linear equation

$$AFu = g, \quad (2)$$

where F is the Fourier transform operator, A is an undersampling operator corresponding to the sampled k-space locations, and g is a vector containing the measurement data. Since the solution u represents a 2D image, a certain type of image regularization can be applied to constrain the solution. In this study, as an example, we use tight frame (TF) as a regularization transformation [13] and solve the problem

$$\begin{aligned} &\min_u |Wu|_1, \\ &\text{s.t. } AFu = g, \end{aligned} \quad (3)$$

where W is a TF transform operator. Minimizing the l_1 norm of the transformed image Wu inherently assumed that the solution image u has a sparse representation under the TF transformation. Note that in the solution image, only the region inside the ROI is of our interest. Hence, we only apply the regularization inside the ROI. This optimization problem (3) can be efficiently solved using the alternating direction method of multipliers [14].

C. Simulation studies

To further demonstrate our proposed idea, we first performed a magnet design study. Specifically, we solved an inverse optimization problem with respect to the current pattern inside the two superconducting magnets. The objective function penalized deviation of the magnetic field from the targeted homogeneous field $B_0 = 0.5\ T$ throughout the FOV. A hard constraint was also imposed to ensure the field strength at the LINAC gantry head is tolerable. After that, we selected a volumetric MRI image of a liver cancer patient. For a slice of interest, we first computed the set Ω and then synthesized the acquired signal according to Eq. (1). For the purpose of proof-of-principle, we only considered undersampling along a number of equiangular straight lines passing through the k-space origin. This is also known as projection data acquisition. With the synthesized data, we then reconstructed the image via the model in Eq. (3). For comparison purpose, we also performed reconstruction using the conventional filtered backprojection (FBP) algorithm [15]. Finally, the image quality was evaluated by comparing with the ground truth input MRI image.

III. Results

A. Magnetic field distribution

Fig. 3 presents the spatial distribution of the x and y component of the B_0 field in the xoy plane. The component perpendicular to this plan is zero. The field in 3D space is

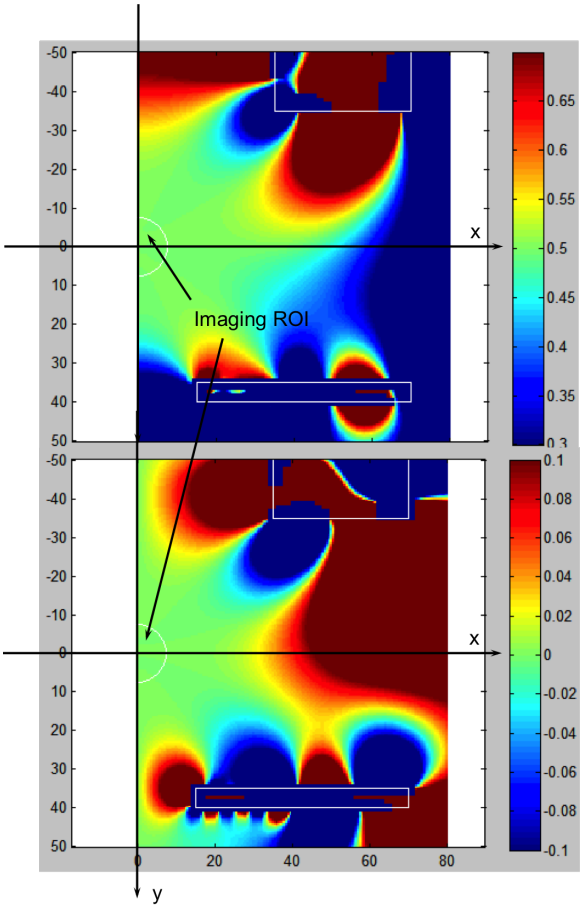

Fig. 3. y (top) and x (bottom) component of the main magnetic field B_0 (T) shown in yox plane. x and y axes are in unit of cm.

rotationally symmetric about the y axis. Using the current optimization technique, the B_0 field was made homogeneous inside the FOV of a diameter of 15 cm with $\Delta B_0/B_0 \sim 50$ ppm. In addition, at the positive direction $y \sim 50$ cm locates the gantry head of a LINAC. The field at this location was constrained to less than 400 $Gauss$, which was expected to be tolerable by a LINAC.

B. Data acquisition

To demonstrate the principle of data acquisition, we assumed a z gradient field with $G_z = 30$ mT/m was applied, and an RF pulse corresponding to the slice at $z_0 = 0$ was used to select this slice. As mentioned above, a set Ω covering this slice inside the ROI, as well as many other points outside the ROI would be selected. This is clearly demonstrated in Fig. 4(a). Those blue voxels are selected voxels inside the 15 cm-diameter ROI that is indicated by the sphere. The voxels formed a slice as expected. In addition, a number of voxels outside the ROI shown in red were also selected.

Because of the magnetic field distribution, the selected voxel outside the ROI did not fall back to the disk region corresponding to the selected slice. This property ensured that the excited signal $\hat{M}(x,y) = \int_{\Omega_{(x,y)}} \mathrm{d}z\, M(x,y,z)$ is identical to the expected signal $M(x,y,z_0)$ inside the ROI. To see this fact more closely, Fig. 4(b) displays the true image $M(x,y,z_0)$ at the slice z_0, whereas the actual excited signal corresponding to an image $\hat{M}(x,y)$ shown in Fig. 4(c). Inside the ROI indicated by the circle, the image $\hat{M}(x,y)$ corresponds to the actual image. In contrast, the part outside the ROI comes from other locations in the 3D space, not even in the slice $z = z_0$.

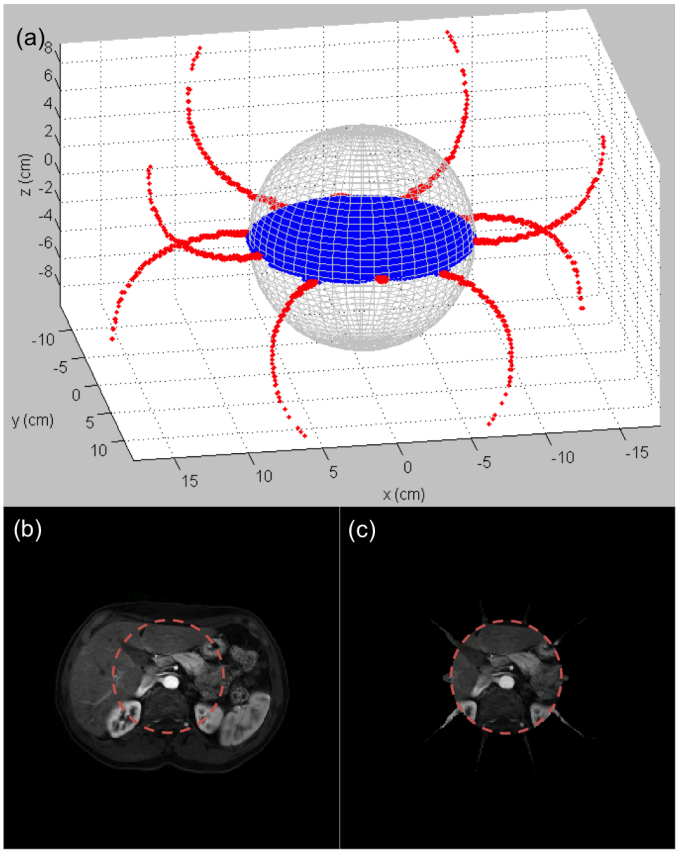

Fig. 4. (a) Voxels excited by an RF pulse corresponding to the slice at $z_0 = 0$ inside the ROI of diameter 15 cm (sphere). Voxels inside the FOV are in blue and those outside the ROI are shown in red. (b) The MRI image $M(x,y,z_0)$ at the slice that is intended to be selected. (c) The actual signal $\hat{M}(x,y)$. Dash circles indicate the region inside the ROI.

C. Imaging reconstruction

With the excitation signal generated, we performed reconstruction using the model in Eq. (3), as well as the conventional FBP algorithm for a comparison purpose. Fig. 5 shows the reconstruction results. With a large number of 360 projections acquired, both the FBP and the iterative algorithm were able to produce high quality images. Again, only the part within the central circular region is of our interest, whereas the part outside should be ignored. When it comes to undersampling cases, streak artifacts start to appear in the FBP results, which is a well known fact for analytical reconstruction algorithms. In contrast, the iterative reconstruction algorithm was still able to maintain image quality to a good extent.

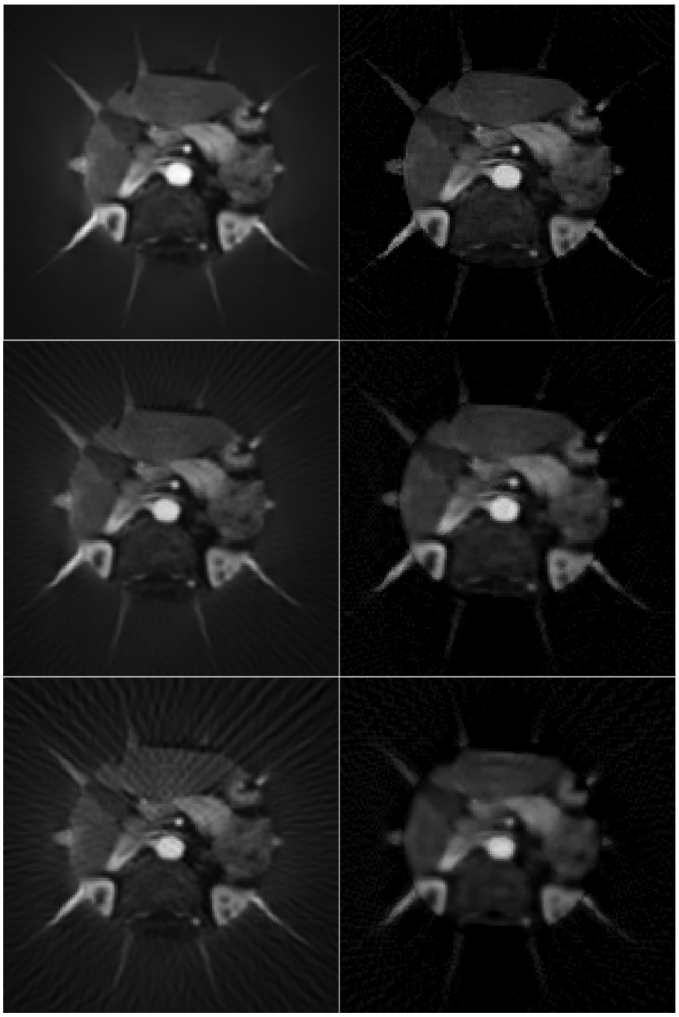

Fig. 5. From top to bottom, the four rows are results reconstructed by using 360, 180, and 120 projections. Left and right columns are results reconstructed using conventional FBP algorithm and the method in Eq. (3).

IV. Discussions

A few discussions are in order. First, the studies shown in this paper are only for the purpose of illustrating the proposed idea. They are by no means the optimal results. To move the proposed idea forward, a number of studies should be followed. For the main magnetic field B_0, they were purely designed through an optimization approach to yield the targeted strength and homogeneity, while maintaining the field strength at the LINAC gantry head to a tolerable level. Yet the field may violate other constraints posed by the LINAC. Hence, further field optimization is needed, e.g. to reduce periphery field strength. A certain type of magnetic shielding will probably be required to further reduce periphery field strength and therefore minimize interference with the LINAC. There are also other factors that we have not considered, such as the impact of multi-leaf-collimator motion, if the iMRI device will be used for imaging during IMRT treatment delivery. All of these will require a substantial amount of work, which will be in our future studies.

The signal excited by the RF pulse comes from both inside the ROI and some regions outside. While this seems to be not a problem in the current study, it posed a challenge in the main magnetic field design: for each slice selected, the set Ω should not contain the part inside the disk region but in other z slices. Otherwise the signal would be picked up by the excitation, and hence compromising the targeted images inside the ROI. There are other possible approaches to overcome this problem. For instance, a time-varying gradient method has been proposed in [16]. The gradient field effectively suppresses signal excitations outside the ROI. In the context of parallel MRI, the use of multiple receiving coils with different spatial sensitive maps may also add additional information to differentiate the true image inside the ROI and that outside.

Recently, a few exciting achievements in the area of compact MRI scanner were reported, which demonstrated the great potential to develop lightweight and LINAC-compatible MRI systems. One notable example is the development from MIT that realized 2D imaging capability in a portable MRI scanner of $< 100\ kg$ in weight [17]. With a rotating spatial encoding method, the system eliminated the needs of gradient coils, substantially reducing system weight and complexity. Extending to 3D imaging capability is under exploration. A system design similar to this is potentially suitable for the integration to the LINAC platform. In our interior tomography framework, a complementary CT image is needed for global imaging, which requires a rotational scan. Hence combining the CT and the MRI data acquisitions in a single gantry rotation is a natural choice. A similar idea has also been proposed in a recent study regarding the combination of CT and MRI systems [18].

This choice, however, limits the system to acquire data only at a zero-degree LINAC couch angle. This fact leads to both advantages and drawbacks. The advantage is relaxed constraint on geometry conflicts between MRI and CT sub-systems. Since the rotational data acquisition has to be performed at zero degree couch angle, geometry constraints with non-zero couch angle setups do not need to be considered anymore. The lightweight system may also allow for a mobile design, which holds the iMRI device on a robotic arm. The device can be docked to the gantry for pre-treatment imaging and removed for treatment delivery. in this way, the non-coplanar treatment capabilities, particularly 4π treatment capability on the current LINAC will not be affected [12]. On the flip side, one drawback of this approach is that 4D imaging during treatment delivery will not be available due to the required rotational data acquisition. Yet the necessity of this function in radiotherapy depends on specific clinical applications. While it is desired to monitor tumor and anatomy motion during a treatment via an imaging approach, using pretreatment MRI image guidance can already ensure targeting accuracy to a large extent. This would be already a significant step forward over the current CBCT-based pre-treatment image guidance. The residual intra-fractional motion can be addressed by using a treatment planning margin, as in the current standard approach.

V. Conclusion

In this paper, we proposed a new concept for MRI-based image guided radiation therapy via an interior tomography approach. We presented initial ideas of the iMRI device design and its integration to a LINAC platform. The device was intended to be made compact, such that it can be retrofit to an existing LINAC system to allow MRI-guided radiation therapy. A few aspects of the system were studied via numerical simulation, including main magnetic field design, signal acquisition, and image reconstruction. The image results were shown in an example to illustrate our idea. The proposed system potentially holds a significant cutting-edge impact over the competing systems in terms of cost, functionality, and potential for clinical translation. Clinical introduction of our system may lead to a profound healthcare impact on cancer treatment by substantially improving treatment accuracy under the MRI-based image guidance.

References

[1] T. Bortfeld, "Imrt: a review and preview," *Physics in Medicine and Biology*, vol. 51, no. 13, p. R363, 2006. [Online]. Available: http://stacks.iop.org/0031-9155/51/i=13/a=R21

[2] D. W. Miller, "A review of proton beam radiation therapy," *Medical Physics*, vol. 22, no. 11, pp. 1943–1954, 1995. [Online]. Available: http://dx.doi.org/10.1118/1.597435

[3] D. A. Jaffray, D. G. Drake, M. Moreau, A. A. Martinez, and J. W. Wong, "A radiographic and tomographic imaging system integrated into a medical linear accelerator for localization of bone and soft-tissue targets," *International Journal of Radiation Oncology*Biology*Physics*, vol. 45, no. 3, pp. 773 – 789, 1999. [Online]. Available: http://www.sciencedirect.com/science/article/pii/S0360301699001182

[4] S. Mutic and J. F. Dempsey, "The viewray system: Magnetic resonanceguided and controlled radiotherapy," *Seminars in Radiation Oncology*, vol. 24, no. 3, pp. 196 – 199, 2014, magnetic Resonance Imaging in Radiation Oncology. [Online]. Available: http://www.sciencedirect.com/science/article/pii/S1053429614000253

[5] J. J. W. Lagendijk, M. van Vulpen, and B. W. Raaymakers, "The development of the mri linac system for online mri-guided radiotherapy: a clinical update," *Journal of Internal Medicine*, vol. 280, no. 2, pp. 203–208, 2016. [Online]. Available: http://dx.doi.org/10.1111/joim.12516

[6] B. G. Fallone, "The rotating biplanar linacmagnetic resonance imaging system," *Seminars in Radiation Oncology*, vol. 24, no. 3, pp. 200 – 202, 2014, magnetic Resonance Imaging in Radiation Oncology. [Online]. Available: http://www.sciencedirect.com/science/article/pii/S1053429614000289

[7] P. J. Keall, M. Barton, and S. Crozier, "The australian magnetic resonance imaginglinac program," *Seminars in Radiation Oncology*, vol. 24, no. 3, pp. 203 – 206, 2014, magnetic Resonance Imaging in Radiation Oncology. [Online]. Available: http://www.sciencedirect.com/science/article/pii/S1053429614000320

[8] G. Wang and H. Yu, "The meaning of interior tomography," *Physics in Medicine and Biology*, vol. 58, no. 16, p. R161, 2013. [Online]. Available: http://stacks.iop.org/0031-9155/58/i=16/a=R161

[9] M. Poole, P. Weiss, H. S. Lopez, M. Ng, and S. Crozier, "Minimax current density coil design," *Journal of Physics D: Applied Physics*, vol. 43, no. 9, p. 095001, 2010.

[10] D. Homa, Y. Liang, C. Hill, G. Kaur, and G. Pickrell, "Superconducting tin core fiber," *Applied Physics A*, vol. 118, no. 1, pp. 23–26, 2015. [Online]. Available: http://dx.doi.org/10.1007/s00339-014-8869-2

[11] D. Homa, G. Kaur, G. Pickrell, and Y. Liang, "Efficient cooling of superconducting fiber core via holey cladding," *Cryogenics*, vol. 61, pp. 25 – 30, 2014. [Online]. Available: http://www.sciencedirect.com/science/article/pii/S0011227514000253

[12] P. Dong, P. Lee, D. Ruan, T. Long, E. Romeijn, D. Low, P. Kulelian, J. Abraham, Y. Yang, and K. Sheng, "4π noncoplanar stereotactic body radiation therapy for centrally located or larger lung tumors," *International Journal of Radiation Oncology Biology Physics*, vol. 86, no. 3, pp. 406–417, 2013.

[13] X. Jia, B. Dong, Y. Lou, and S. B. Jiang, "Gpu-based iterative cone-beam ct reconstruction using tight frame regularization," *Physics in Medicine and Biology*, vol. 56, no. 13, p. 3787, 2011. [Online]. Available: http://stacks.iop.org/0031-9155/56/i=13/a=004

[14] S. Boyed, N. Parikh, E. Chu, B. Peleato, and J. Eckstein, "Distributed optimization and statistical learning via the alternating direction method of multipliers," *Foundation and Trends in Machine Learning*, vol. 3, no. 1, pp. 1–122, 2011.

[15] L. D. L.A. Feldkamp and J. Kress, "Practical cone-beam algorithm," *Journal of the Optical Society of America A*, vol. 1, no. 6, pp. 612–619, 1984.

[16] G. Wang, J. Zhang, H. Gao, V. Weir, H. Yu, W. Cong, X. Xu, H. Shen, J. Bennett, M. Furth *et al.*, "Towards omni-tomographygrand fusion of multiple modalities for simultaneous interior tomography," *PloS one*, vol. 7, no. 6, p. e39700, 2012.

[17] C. Z. Cooley, J. P. Stockmann, B. D. Armstrong, M. Sarracanie, M. H. Lev, M. S. Rosen, and L. L. Wald, "Two-dimensional imaging in a lightweight portable mri scanner without gradient coils," *Magnetic Resonance in Medicine*, vol. 73, no. 2, pp. 872–883, 2015. [Online]. Available: http://dx.doi.org/10.1002/mrm.25147

[18] L. Gjesteby, Y. Xi, M. Kalra, Q. Yang, and G. Wang, "Hybrid imaging system for simultaneous spiral mr and x-ray (mrx) scans," *IEEE Access*, vol. PP, no. 99, pp. 1–1, 2016.